

Reliable OFDM Transmission with Ultra-Low Resolution ADC

Hanqing Wang, Wan-Ting Shih, Chao-Kai Wen, and Shi Jin

arXiv:1801.00893v1 [cs.IT] 3 Jan 2018

Abstract—The use of low-resolution analog-to-digital converters (ADCs) can significantly reduce power consumption and hardware cost. However, severe nonlinear distortion due to low-resolution ADCs makes achieving reliable data transmission challenging. Particularly, for orthogonal frequency division multiplexing (OFDM) transmission, the orthogonality among subcarriers is destroyed, which invalidates the conventional linear receivers that highly relies on this orthogonality. In this study, we develop an efficient *system architecture* for OFDM transmission with ultra-low resolution ADC (e.g., 1–2 bits). A novel channel estimator is proposed to estimate the desired channel parameters without their priori distributions. In particular, we integrate the linear minimum mean squared error channel estimator into the generalized Turbo (GTurbo) framework and derive its corresponding extrinsic information to guarantee the convergence of the GTurbo-based algorithm. We also propose feasible schemes for automatic gain control, noise power estimation, and synchronization. Furthermore, we construct a proof-of-concept prototyping system and conduct over-the-air (OTA) experiments to examine the feasibility/reliability of the entire system. To the best of our knowledge, this is the first work that focused on system design and implementation of communications with low-resolution ADCs worldwide. Numerical simulation and OTA experiment results demonstrate that the proposed system supports reliable OFDM data transmission with ultra-low resolution ADCs.

Index Terms—Low-precision ADC, OFDM, Turbo signal recovery, prototyping system.

I. INTRODUCTION

Achieving highly reliable data transmission with low hardware cost and low power consumption is a substantial pursuit of future wireless communication systems. Applying ultra-low resolution (i.e., 1–2 bit) quantizers, including analog-to-digital converters (ADCs) or digital-to-analog converters (DACs) is a promising solution that has been widely explored by the academia and industry. The advantages of low-resolution quantizers can be summarized as follows.

- The relationship of power consumption of the quantizer with its quantization precision b and sampling frequency F_s expressed by $P_{\text{ADC}} \propto 2^b \times F_s$ [1] reveals that the reduction in quantizers' precision can lead to the exponential decrease in their power consumption.
- Data represented by few bits can be easily stored and transferred, which allows for relaxing the quality requirements on the radio frequency (RF) and interface circuits.

H. Wang and S. Jin are with the National Mobile Communications Research Laboratory, Southeast University, Nanjing 210096, P. R. China. P (e-mail: hqwanglyt@seu.edu.cn; jinshi@seu.edu.cn).

W.-T. Shih and C.-K. Wen are with the Institute of Communications Engineering, National Sun Yat-sen University, Kaohsiung, Taiwan (e-mail: sydney2317076@gmail.com; chaokai.wen@mail.nsysu.edu.tw).

- The cost and implementation complexity of low-resolution quantizers are extremely low [2].

The feasibility of using low-resolution quantizers has been demonstrated by those studies that analyze the capacity or achievable rate degradation caused by low-resolution quantizers [3]–[9]. For example, as shown by the capacity derivation for additive white Gaussian noise (AWGN) channel in [4], only 10%–20% capacity is lost under the quantization precision of 2–3 bits. Research in [7] revealed that in a multiple antenna array system, equipping only a small proportion of high-resolution ADCs can closely approximate the achievable rate of conventional architecture with all full-resolution ADCs. These results have inspired subsequent studies into transceiver designs.

Several algorithms have been developed for flat-fading MIMO or massive MIMO systems with low-resolution ADCs, such as linear receiver [10], [11], relaxed convex optimization based algorithm [12], coding theory-based approach [13], and supervised learning based method [14]. For the coarsely quantized MIMO systems with channel matrix comprising i.i.d. Gaussian entries, an iterative process called generalized approximate message passing (GAMP) can be strictly proven to yield Bayesian optimal detection or estimation performance [15]–[17]. However, these studies lack at least two important aspects. First, linear receivers yield acceptable performance due to the array gain from a large number of received data streams. This compensates for performance loss caused by low-resolution quantizers to a large extent, which weakens the contribution of subsequently developed algorithms with better performance but higher complexity. Second, the aforementioned works did not consider the wideband channel, which is a typical setting of future communication systems.

For the wideband channel, the delay spread is generally larger than the symbol duration of the transmitted signal, which leads to severe frequency-selective fading and serious inter-symbol interference (ISI). Orthogonal frequency division multiplexing (OFDM) is a well-developed multicarrier transmission technology, which enables the decomposition of the ISI channel into a bank of orthogonal flat-fading subchannels [18]. Therefore, the OFDM waveform has been widely used by various wideband wireless communication systems to pursue high data rates, such as IEEE 802.11ad [19] and 5G air interface. OFDM transmissions combined with low-resolution quantizers (hereinafter referred to as quantized OFDM (Q-OFDM) systems) are considered a typical setting for future communication systems. Works for designing Q-OFDM receivers have emerged, such as linear receiver [20] and fast adaptive shrinkage/thresholding algorithm [21]. Their

suboptimality is due to the neglect of nonlinear distortion caused by coarse quantization and the relaxation of detected symbols from discrete constellation to the Gaussian signal. In [22], the GAMP is mechanically applied to the detection and channel estimation problem for a quantized MIMO-OFDM system. However, GAMP has only been proven optimal for the i.i.d. Gaussian linear transformation matrix but not for the orthogonal matrix of our interest. The Bayesian optimal detector for the Q-OFDM system has been proposed and theoretically proven in [23].

This paper aims to make breakthrough progress in terms of practical feasibility of reliable data transmission based on low-resolution quantizers given that majority of extant works merely remain theoretic and simulation-based. Their numerical simulation results seem to verify the feasibility of employing low-resolution quantizers but fail to eliminate the widespread doubts regarding the application of reliable data transmission with low-resolution quantizers in practice. Therefore, further research should be conducted for system design and implementation. Current works have proven that iterative processes and complicated nonlinear computations involved in signal recovery or algorithm formation for combating strong nonlinear distortion can be implemented hardware-friendly. The feasible hardware architecture of generalized Turbo (GTurbo) for coarsely quantized compressed sensing problem was first presented in [24], wherein a hardware-friendly approximation for probability distribution functions, and the pipelined and folding hardware architecture, are proposed. These architectures have been proven to exhibit only a slight performance degeneration compared with the original full-precision result. In addition, in [25], massively parallel very-large-scale integrated architectures were developed for massive MIMO downlink with 1-bit DACs, which achieved excellent error-rate performance under acceptable hardware complexity, system cost, and circuit power consumption.

Efficient hardware architecture design is the first and most important step. However, achieving reliable data transmission with low-resolution quantizers is an extensive and complicated process. The preceding related works mentioned only focused on developing a certain algorithm for signal recovery instead of the overall system design to guarantee the practicability of these algorithms. Specifically, under strong nonlinear distortion, maintaining the input signal amplitude within a certain range (i.e., automatic gain control (AGC)), estimating the noise power, and identifying the starting point of each radio frame are challenging tasks. To the best of our knowledge, no previous work has accounted for the preceding issues mentioned, thereby motivating us to address the problem. In this paper, we not only propose a feasible channel estimator and data detector but also introduce a series of robust solutions for AGC, noise estimation, and synchronization, which constitute the entire system architecture.

Our ultimate goal is not restricted to propose a seemingly feasible system architecture but to implement the first prototyping system in the world for verifying the data transmission reliability using low-resolution ADCs through over-the-air (OTA) experiments. We focus on achieving wideband high-speed OFDM transmission under the extreme case of 1-bit

quantization. Intuitively, under AWGN channel, when the precision of ADC is equal to the number of bits per real dimension of the employed modulation scheme, the achievable error-rate performance is equivalent to the performance under full-resolution quantization. For example, 1-bit quantization is adequate for the transmission of 4-QAM symbols under AWGN channel. However, for OFDM transmission where the inverse discrete Fourier transform (IDFT) operation produces continuous time-domain samples instead of discrete constellations, a high ADC precision is expected for reliable signal recovery. The OTA experiment results reveal that the preceding intuitive knowledge is also valid for OFDM systems, that is, 1-bit quantization can support OFDM transmission of 4-QAM symbols. Experiments are further conducted for the transmission of 16-QAM under 2-bit quantization, whose reliability is also proven.

The rest of paper is organized as follows. Section II models the inference problem considered in this study and highlights the challenges caused by coarsely quantized received signal. Section III presents the overall receiver architecture and provides detailed explanations on each processing module. Numerical simulation results are shown in Section IV for the performance evaluations and comparisons of the proposed algorithms. Section V introduces the prototyping system and presents the OTA experiment results. Finally, Section VI concludes this paper.

Notations: This paper uses lowercase and uppercase bold-face letters to represent vectors and matrices, respectively. For vector \mathbf{a} , a_j denotes the j -th entry of \mathbf{a} , and the operator $\text{diag}(\mathbf{a})$ denotes the diagonal matrix with diagonal elements as the entries of \mathbf{a} . Moreover, the real and imaginary parts of a complex scalar a are represented by a^R and a^I , respectively. The distribution of a proper complex Gaussian random variable z with mean μ and variance ν is expressed by

$$z \sim \mathcal{CN}(z; \mu, \nu) = \frac{1}{\pi\nu} e^{-\frac{|z-\mu|^2}{\nu}}.$$

Similarly, $\mathcal{N}(z; \mu, \nu)$ denotes the probability density function of a real Gaussian random variable z with mean μ and variance ν . Let Dz denote the real Gaussian integration measure

$$Dz = \phi(z)dz \text{ with } \phi(z) = \frac{1}{\sqrt{2\pi}} e^{-\frac{z^2}{2}}.$$

The cumulative Gaussian distribution function is defined as $\Phi(z) = \frac{1}{\sqrt{2\pi}} \int_{-\infty}^z e^{-\frac{t^2}{2}} dt$, and the Q function is defined as $Q(z) = 1 - \Phi(z)$.

II. SYSTEM MODEL AND CHALLENGES

We consider the overall system architecture design for supporting reliable data transmission with OFDM technique based on ultra-low resolution ADC (i.e., 1–2 bit) at the receiver. The OFDM system comprises N orthogonal subcarriers. Among them, only N_d subcarriers corresponding to the frequency $-\frac{N_d F_s}{2 N}, \dots, -\frac{F_s}{N}, \frac{F_s}{N}, \dots, \frac{N_d F_s}{2 N}$ are dedicated to data transmission, where F_s denotes the sampling frequency. Meanwhile, other $N - N_d$ subcarriers are reversed as guard band, which are padded by the null signal to reduce the signal leakage into the sidelobe. In this paper, we use $\mathcal{X} =$

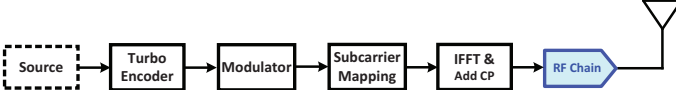


Fig. 1: Block diagram of an OFDM transmitter.

$\{1, 2, \dots, N\}$ to denote the index set of all subcarriers and $\mathcal{X}_d \subseteq \mathcal{X}$ to denote the index subset of the N_d subcarriers used for data transmission. In addition, the subscript “ d ” for N -dimension vector and a matrix with N rows (for example, \mathbf{a}_d and \mathbf{A}_d) represent the N_d -dimension subvector comprised of the elements of \mathbf{a} with index \mathcal{X}_d and the submatrix comprised of the rows of \mathbf{A} with index \mathcal{X}_d , respectively.

The signaling process at the transmitter follows the conventional OFDM transmission, which is shown in Fig. 1. The information bits generated by the data source are first encoded using Turbo code. Then, the modulator maps the coded bits into corresponding constellation symbols based on the selected modulation method, such as M -ary quadrature amplitude modulation (M -QAM), and each modulated symbol is assigned into one of N_d subcarrier of the OFDM symbol. We denote the vector of frequency-domain constellation symbols as $\mathbf{s} \in \mathbb{C}^{N \times 1}$, where $s_j = 0$ for $j \in \mathcal{X} \setminus \mathcal{X}_d$. Subsequently, the frequency-domain OFDM symbol \mathbf{s} is transformed into the time-domain using N -point IDFT. The CP with length L_{cp} larger than the maximum length of channel impulse response is appended at the beginning of the OFDM symbol to avoid the ISI due to the multipath effect of wireless channel. The baseband sequence is finally fed into the RF chain to be up-converted and transmitted over the wireless channel.

At the receiver, the RF received signal is first down-converted into the analog baseband. The equivalent baseband received signal is sampled and quantized using ultra-low resolution ADC. After CP removal and under ideal synchronization, the coarsely quantized time-domain samples of an OFDM symbol can be expressed by a vector

$$\mathbf{q} = \mathcal{Q}_c(\sqrt{g_{\text{AGC}}} (\mathbf{F}^H \text{diag}(\mathbf{h}) \mathbf{s} + \mathbf{n})), \quad (1)$$

where \mathbf{F} denotes the normalized DFT matrix with $\frac{1}{\sqrt{N}} e^{-2\pi j(n-1)(m-1)/N}$ being its (m, n) -th entry; $\mathbf{n} \in \mathbb{C}^{N \times 1}$ denotes the AWGN vector with distribution $\mathcal{CN}(0, \sigma^2 \mathbf{I})$; \mathbf{h} is the vector of frequency-domain channel gains, which is obtained by operating DFT on the time-domain tapped delay line representation of the ISI channel denoted by $\mathbf{h}_t = [h_{t,1}, h_{t,2}, \dots, h_{t,N}]^T$ with $h_{t,j} = 0$ for $(L+1) \leq j \leq N$ with L being the maximum number of channel taps; g_{AGC} is the temporal gain of the AGC unit used for adjusting the input amplitude of ADC within a certain range; $\mathcal{Q}_c(\cdot)$ denotes the mapping function of the elementwise complex-valued quantizer. The complex-valued quantizer comprises two parallel real-valued B -bit quantizers $\mathcal{Q}(\cdot)$ that separately and independently quantize the real and imaginary parts of each analog input sample. For a scalar analog input y ,

$$\mathcal{Q}_c(y) = \mathcal{Q}(y^R) + j\mathcal{Q}(y^I),$$

where the quantizer $\mathcal{Q}(\cdot)$ outputs the discrete value c_b when the real-valued input y^R or y^I is within the interval $(r_{b-1}, r_b]$,

$-\infty = r_0 < r_1 < \dots < r_{2B-1} < r_{2B} = \infty$ are the thresholds, and c_b is taken as the centroid of the interval $(r_{b-1}, r_b]$.

The receiver is designed for recovering the original information bits from coarse quantization observation \mathbf{q} with minimum error rate. The canonical solution is to compute a certain estimate of \mathbf{s} and its corresponding mean-square error for subsequently calculating the log-likelihood ratio (LLR) corresponding to each coded bit, which is finally fed into the Turbo decode to recover information bits. Many issues should be considered for receiver design to ensure the performance of this information recovery process. We summarize the challenges as follows:

1) *AGC and noise power estimation*: AGC and noise power estimation are two essential components in modern digital communications. In conventional systems with full-resolution ADCs, these functional modules are based on the power accumulator performed by taking the long-term time average of the amplitude of the corresponding received baseband samples. However, almost all amplitude information has already been lost due to the low-resolution ADCs. Therefore the first challenging issue is how to design the certain architecture in receiver to overcome the loss of signal amplitude and further facilitate AGC and noise power estimation.

2) *Synchronization*: The classical method of synchronization searching is based on transmitting a pre-defined complex sequence at the beginning of each radio frame. At the receiver, we compute the correlation between the received and reference sequence and find the local maximum correlation to identify the starting point of each frame. It is desirable to clarify the validity of this method under coarsely quantized received samples, and more important, to design a specialized reference sequence to guarantee the synchronization accuracy.

3) *Channel estimation*: A common approach to obtaining the CSI is to periodically transmit pilot signals at frequency domain, which are contained by subcarriers with index \mathcal{X}_d . The vector of frequency-domain pilot symbols is denoted by $\mathbf{p} \in \mathbb{C}^N$, where $p_j = 0$ for $j \in \mathcal{X} \setminus \mathcal{X}_d$. The quantized received signal vector for each pilot OFDM symbol is given by

$$\mathbf{q} = \mathcal{Q}_c(\sqrt{g_{\text{AGC}}} \mathbf{F}^H \text{diag}(\mathbf{p}) \mathbf{h} + \mathbf{n}), \quad (2)$$

and we define an auxiliary vector as $\bar{\mathbf{p}} = \sqrt{g_{\text{AGC}}} \mathbf{p}$ to simplify the notation. Conventional linear channel estimator first perform the least-square (LS) channel estimation to yield $\mathbf{F}\mathbf{q}/\bar{\mathbf{p}}$, and then left-multiplies it by a certain weight matrix. This method is initially derived based on the orthogonality among different subcarriers. However, this orthogonality has not been preserved due to the low-resolution ADC. This motivates us to re-design a specialized channel estimator for estimating \mathbf{h}_d from (2).

4) *Data detection*: Data detector aims to compute the estimate of each frequency-domain modulated symbol based on \mathbf{q} and the estimated CSI $\bar{\mathbf{h}}$. The conventional OFDM receiver transforms the quantized signal \mathbf{q} into frequency-domain and yields $\tilde{\mathbf{q}} = \mathbf{F}\mathbf{q}$, which is followed by the one-tap equalizer. The receiver computes the estimate of s_j for $j \in \mathcal{X}_d$ by \tilde{q}_j/\bar{h}_j , and their corresponding mean squared error (MSE) by $g_{\text{AGC}}\bar{\sigma}^2/\bar{h}_j$, where $\bar{\sigma}^2$ denotes the estimated noise power. For full-precision quantization, the DFT operation on \mathbf{q} enables

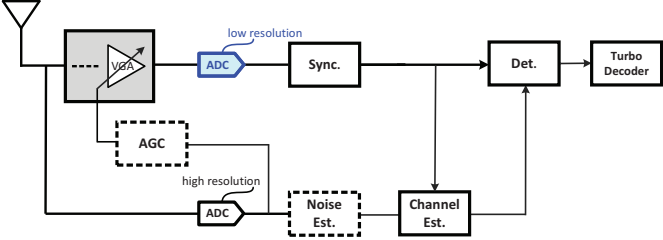


Fig. 2: Receiver architecture.

each \tilde{q}_j to be an AWGN observation of $h_j s_j$ corresponding to the j -th subcarrier. However, this conventional OFDM detector can no longer yield acceptable performance for the low-resolution quantization case because the orthogonality among subcarriers has been severely destroyed.

III. RECEIVER ARCHITECTURE

In this section, we introduce the overall architecture of the proposed receiver, and provide detailed explanations on each processing module. In this section, we first introduce the overall architecture of the proposed receiver, and then give detailed explanations about how each processing modules work. Once the RF signal is received from the wireless channel, it is down-converted into the analog baseband for the subsequent processing. The overall architecture of baseband processing at the receiver is shown as block diagram in Fig. 2. The received analog baseband signal is divided into two streams to be independently sampled and discretized for different purposes to facilitate digital storage and processing. One stream is quantized with ultra-low resolution (e.g., 1–2 bit) and sampled with frequency F_s , from which synchronization searching, channel estimation and data detection are sequentially conducted. Another stream is quantized with high precision but sampled with low sampling frequency (tens or hundreds times lower than F_s), which is used for signal/noise power accumulator to assist AGC and noise power estimation. We elaborate the details on each processing module in the following subsections.

A. AGC and Noise Power Estimation

The AGC unit prior to the low-resolution ADC is used to adjust the amplitude of baseband signal within a certain range to suit the fixed thresholds of the ADC, which is indispensable for the quantization resolution of 2 bit and more. In our system, AGC is implemented by measuring the average power of each received radio frame P_r and normalizing it to be one, hence $g_{AGC} = 1/P_r$. For 1-bit quantization, the AGC itself is not necessary. However, the average power of received signal P_r is a requisite parameter in this case for the initialization of proposed iterative algorithms and the recovery of the channel norm. Considering the development of a unified system architecture for different quantization resolutions, we reserve the AGC module to obtain P_r by taking the reciprocal of g_{AGC} when 1-bit ADC is used.

The noise power estimation is conducted by assigning a few OFDM symbols in each frame to transmit null signal and

measuring the average power of these OFDM symbols at the receiver. The signal/noise power is measured by using the samples quantized by the *high-resolution* ADC with low sampling frequency. Notably, this assistant high-resolution ADC will not lead to significant increase in power consumption under a significantly low sampling frequency. The reduction in the precision of signal/noise power estimation due to sampling frequency reduction can be compensated by prolonging the time of power accumulator.

B. Synchronization

We perform the symbol-timing synchronization at the receiver to precisely identify the starting point of each frame from the sequence of coarsely quantized samples. Owing to the low cross-correlation and high autocorrelation, the Zadoff-Chu (ZC) sequence is selected as the primary synchronization sequence (PSS). For the OFDM symbols in each frame arranged to transmit PSS, the ZC sequence is placed at 62 subcarriers on both sides of the zero frequency, while other subcarriers are padded by null signal to facilitate accurate synchronization. The synchronization searching is conducted by calculating the correlation between the quantized received sequence and a reference sequence and determining the position with highest correlation to identify the starting point of each frame. We redesign the reference sequence considering the effect of low-resolution ADC as the following steps:

- 1) Transferring the frequency-domain OFDM symbol transmitting PSS into time-domain.
- 2) Normalizing the power of the resulting sequence.
- 3) Discretizing the obtained sequence by using the mapping function $\mathcal{Q}_c(\cdot)$.

Once the starting point of each frame is identified, the CP of each OFDM symbol is removed, and quantized time-domain OFDM symbols are inputted into their corresponding processing modules, that is, channel estimator or detector.

C. Channel Estimator

The goal of channel estimator is to estimate the frequency-domain channel parameters of those subcarriers dedicated for data transmission, namely \mathbf{h}_d , based on the given \mathbf{q} and $\bar{\mathbf{p}}$. The estimated channel parameter $\bar{\mathbf{h}}_d$ is subsequently utilized as the CSI for data detection by applying Algorithm 2 to the remainder of OFDM symbols in the current slot. Before formally introducing the proposed algorithm, we define the following two auxiliary vectors

$$\mathbf{x} = \text{diag}(\bar{\mathbf{p}})\mathbf{h}, \quad \mathbf{z} = \mathbf{F}^H \mathbf{x} \quad (3)$$

to facilitate our subsequent discussion. Herein, \mathbf{x} and \mathbf{z} represent the noiseless received signal in frequency and time domain, respectively.

The channel estimation problem (2) has been formulated as a generalized linear model of the frequency-domain channel vector \mathbf{h} . A straightforward idea to estimate \mathbf{h}_d is to directly apply the GTurbo principle [26] proposed for quantized compressed sensing problem with orthogonal measurement matrix to (2). The GTurbo-based algorithm comprises two processing

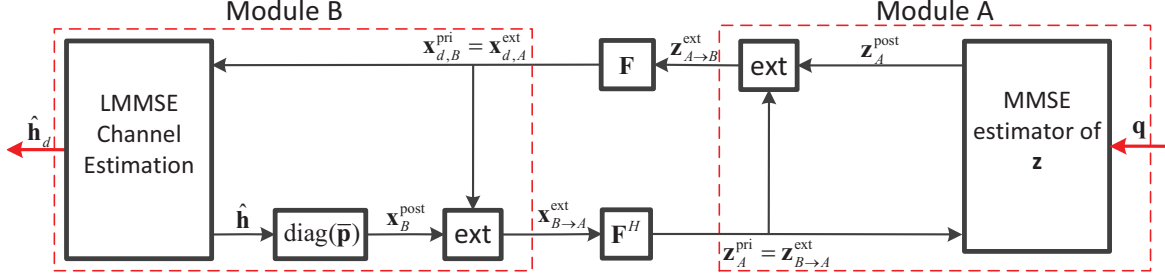


Fig. 3: Block diagram of GTurbo-LMMSE channel estimator. The “ext” block represents the extrinsic information computation. The block of a certain matrix represents the operation of left-multiplying the input vector by the matrix in the block.

modules: Module A is used to directly produce a coarse estimation of \mathbf{x} from the quantized measurement \mathbf{q} , which is equivalent to produce a coarse estimate of \mathbf{h} following the linear transform in (3); Module B is used to produce a refined version of the estimated \mathbf{h}_d by computing its minimum MSE (MMSE) estimate. The extrinsic mean and variance of each module are passed to the other module as the input. The estimate of \mathbf{h}_d is successively refined by iteratively executing the two modules until convergence. However, Module B of the GTurbo-based algorithm, which computes the MMSE estimate of \mathbf{h}_d , requires the prior distribution of the channel parameters. The statistics of wireless channels are unavailable, hence the use of the GTurbo-based algorithm for the channel estimation problem is invalid.

The extant GTurbo framework should be extended to accommodate the inference problem without the priori distribution of the parameters to be estimated. The challenges encountered in the channel estimation algorithm design include:

- The re-design of Module B to directly extract the desired channel parameter \mathbf{h}_d from its input without using the the priori distribution of \mathbf{h}_d .
- The derivation of extrinsic mean and variance corresponding to the preceding operations guarantee the convergence of the proposed algorithm.

The unavailability of the prior distribution of \mathbf{h} makes the Bayesian optimal MMSE estimation infeasible, thereby significantly complicating the algorithm design. However, the breakthrough can be completed given the decoupling effect of Module A. Specifically, the output of Module A, which is also the input of Module B, can be approximated by the element-wise product of the pilot vector and the frequency-domain channel response vector corrupted by the AWGN. Module B is tasked to extract the channel parameter \mathbf{h}_d through its AWGN observation, which can be resorted to the well-developed denoiser in the field of image processing. Various kinds of denoisers are available, such as the SURE-LET [27], BM3D [28], dictionary learning [29], and SVT [30]. However, these denoisers are specialized for i.i.d. sparse signal, low-rank matrix, or image. In our earlier trial computer simulations, we find that mechanical application of these denoisers cannot yield satisfactory performance for the estimation of \mathbf{h}_d with strongly correlated entries. Therefore, we must select a new kind of denoiser for this channel estimation problem.

We observe that extracting \mathbf{h}_d from its approximate AWGN

Algorithm 1: GTurbo-LMMSE Channel Estimator

Initialization: $\mathbf{z}_A^{\text{pri}} = \mathbf{0}_{N \times 1}$, $\mathbf{x}_B^{\text{pri}} = \mathbf{0}_{N \times 1}$, $\mathbf{x}_B^{\text{post}} = \mathbf{0}_{N \times 1}$,

$$v_A^{\text{pri}} = 1 - g_{AGC}\sigma^2;$$

for $t = 1 : T_{\max}$ **do**

Module A:

(1) Compute the a posteriori mean/variance of \mathbf{z} :

$$z_{j,A}^{\text{post}} = \mathbb{E} [z_j^R | q_j^R] + j\mathbb{E} [z_j^I | q_j^I], \quad (4a)$$

$$v_{j,A}^{\text{post}} = \text{var} [z_j^R | q_j^R] + \text{var} [z_j^I | q_j^I], \quad (4b)$$

(2) Compute the extrinsic information of Module A:

$$v_A^{\text{post}} = \frac{1}{N} \sum_{j=1}^N v_{j,A}^{\text{post}}, \quad (5a)$$

$$v_B^{\text{pri}} = v_{A \rightarrow B}^{\text{ext}} = \left(\frac{1}{v_A^{\text{post}}} - \frac{1}{v_A^{\text{pri}}} \right)^{-1}, \quad (5b)$$

$$\mathbf{x}_A^{\text{ext}} = v_{A \rightarrow B}^{\text{ext}} \left(\frac{\mathbf{F} \mathbf{z}_A^{\text{post}}}{v_A^{\text{post}}} - \frac{\mathbf{F} \mathbf{z}_A^{\text{pri}}}{v_A^{\text{pri}}} \right), \quad (5c)$$

$$\mathbf{x}_{d,B}^{\text{pri}} = \mathbf{x}_{d,A \rightarrow B}^{\text{ext}}, \quad (5d)$$

Module B:

(3) LMMSE channel estimation:

$$\hat{\mathbf{h}} = \mathbf{W}_{\text{LMMSE}} \text{diag}^{-1}(\bar{\mathbf{p}}_d) \mathbf{x}_{d,B}^{\text{pri}}, \quad (6)$$

(4) Compute the extrinsic information of Module B:

$$\mathbf{x}_{d,B}^{\text{post}} = \text{diag}(\bar{\mathbf{p}}_d) \hat{\mathbf{h}}_d, \quad (7a)$$

$$\mathbf{x}_A^{\text{pri}} = \mathbf{x}_{B \rightarrow A}^{\text{ext}} = c \left(\mathbf{x}_B^{\text{post}} - \alpha \mathbf{x}_B^{\text{pri}} \right), \quad (7b)$$

$$\mathbf{z}_A^{\text{pri}} = \mathbf{F}^H \mathbf{x}_A^{\text{pri}}, \quad (7c)$$

$$v_A^{\text{pri}} = v_{B \rightarrow A}^{\text{ext}} = \frac{\|\mathbf{x}_{d,B}^{\text{ext}} - \mathbf{x}_{d,B}^{\text{post}}\|^2}{N_d}. \quad (7d)$$

end

observation is similar to channel estimation problem in the conventional full-resolution OFDM systems. Many robust channel estimators are available for being selected as the denoiser here. Among these channel estimators, linear MMSE (LMMSE) channel estimator is a type of widely-used linear channel estimator, which is aimed at minimizing the MSE. The reliability and hardware efficiency of the LMMSE channel estimator are confirmed by our previously developed massive MIMO-OFDM prototyping system [31]. Therefore, we select

the LMMSE channel estimator as the denoiser in Module B. The proposed algorithm is definitely named as GTurbo-LMMSE channel estimator.

The proposed channel estimation algorithm is presented in Algorithm 1, and its computation procedure is illustrated in Fig. 3. We then provide several intuitive explanations to allow readers to improve their understanding of the proposed channel estimator. In Module A, (4a) and (4b) compute the MMSE estimate of z_j under the given quantized observation q_j , and its corresponding MSE, where $E[z_j^R | q_j^R]$ and $\text{var}[z_j^R | q_j^R]$ denote the posteriori expectation and variance of z_j^R given q_j^R under the assumption of $P(z_j^R) = \mathcal{N}(z_j^R, z_{j,A}^{\text{pri},R}, \frac{1}{2}v_A^{\text{pri}})$. Their explicit expressions can be derived through [17] as

$$E[z_j^R | q_j^R] = z_{j,A}^{\text{pri},R} + \frac{v_A^{\text{pri}}}{\sqrt{2(v_A^{\text{pri}} + \sigma^2)}} \left(\frac{\phi(\eta_1) - \phi(\eta_2)}{\Phi(\eta_1) - \Phi(\eta_2)} \right), \quad (8a)$$

$$\text{var}[z_j^R | q_j^R] = \frac{v_A^{\text{pri}}}{2} - \frac{(v_A^{\text{pri}})^2}{2(v_A^{\text{pri}} + \sigma^2)} \times \left[\left(\frac{\phi(\eta_1) - \phi(\eta_2)}{\Phi(\eta_1) - \Phi(\eta_2)} \right)^2 + \frac{\eta_1\phi(\eta_1) - \eta_2\phi(\eta_2)}{\Phi(\eta_1) - \Phi(\eta_2)} \right], \quad (8b)$$

where $\sigma^2 = g_{\text{AGC}}\widehat{\sigma^2}$, and

$$\eta_1 = \frac{z_{j,A}^{\text{pri},R} - u(q_j^R)}{\sqrt{(v_A^{\text{pri}} + \sigma^2)/2}}, \quad \eta_2 = \frac{z_{j,A}^{\text{pri},R} - l(q_j^R)}{\sqrt{(v_A^{\text{pri}} + \sigma^2)/2}} \quad (9)$$

where $l(q_j^R)$ and $u(q_j^R)$ are the lower and upper bounds corresponding to the quantizer output value q_j^R . Moreover, $E[z_j^I | q_j^I]$ and $\text{var}[z_j^I | q_j^I]$ can be similarly computed by simply replacing $z_{j,A}^{\text{pri},R}$ with $z_{j,A}^{\text{pri},I}$ when computing η_1 and η_2 in (9). Subsequently, extrinsic information of Module A can be computed by (5a)–(5d); specifically, (5a) and (5b) compute the extrinsic variance of Module A, whereas (5c) and (5d) compute the extrinsic mean of Module A, which is then used as the input of Module B.

We then consider the operations of Module B for extracting the desired channel parameters. The input of Module B $\mathbf{x}_B^{\text{pri}}$ can be approximately represented by the AWGN observation of $\mathbf{x} = \text{diag}(\bar{\mathbf{p}})\mathbf{h}$ as follows:

$$\mathbf{x}_B^{\text{pri}} = \text{diag}(\bar{\mathbf{p}})\mathbf{h} + \boldsymbol{\omega}_B, \quad (10)$$

where $\boldsymbol{\omega}_B \sim \mathcal{CN}(\mathbf{0}, v_B^{\text{pri}}\mathbf{I})$. The LMMSE denoiser for extracting \mathbf{h}_d from $\mathbf{x}_B^{\text{pri}}$ is constructed by (6), where $\mathbf{W}_{\text{LMMSE}}$ is the corresponding linear weight matrix with the form

$$\mathbf{W}_{\text{LMMSE}} = \mathbf{R}_{\mathbf{h}\mathbf{h}_d}(\mathbf{R}_{\mathbf{h}_d\mathbf{h}_d} + \gamma^2\mathbf{I}), \quad (11)$$

where parameter γ^2 can be theoretically selected as the signal-to-noise ratio (SNR) of equivalent AWGN channel (10), that is $1/v_B^{\text{pri}}$. The notation $\mathbf{R}_{\mathbf{ab}} = E\{\mathbf{a}\mathbf{b}^H\}$ represents the cross-correlation matrix of vectors \mathbf{a} and \mathbf{b} . The major challenge here is that the exact correlation matrices $\mathbf{R}_{\mathbf{h}\mathbf{h}_d}$ and $\mathbf{R}_{\mathbf{h}_d\mathbf{h}_d}$ are unknown. Therefore, we assume the time-domain profile of the channel to be a uniform tapped delay line with the maximum number of channel taps as \hat{L} . The (m, n) -th entry

of $\mathbf{R}_{\mathbf{h}\mathbf{h}_d}$ and $\mathbf{R}_{\mathbf{h}_d\mathbf{h}_d}$ given this assumption can be computed by [32, Appendix A]

$$\begin{aligned} [\mathbf{R}_{\mathbf{h}\mathbf{h}_d}]_{(m,n)} &= \begin{cases} 1, & m = \mathcal{X}_d(n) \\ \frac{1-e^{-j2\pi\hat{L}\frac{m-\mathcal{X}_d(n)}{N}}}{j2\pi\hat{L}\frac{m-\mathcal{X}_d(n)}{N}}, & m \neq \mathcal{X}_d(n) \end{cases} \\ [\mathbf{R}_{\mathbf{h}_d\mathbf{h}_d}]_{(m,n)} &= \begin{cases} 1, & \mathcal{X}_d(m) = \mathcal{X}_d(n) \\ \frac{1-e^{-j2\pi\hat{L}\frac{\mathcal{X}_d(m)-\mathcal{X}_d(n)}{N}}}{j2\pi\hat{L}\frac{\mathcal{X}_d(m)-\mathcal{X}_d(n)}{N}}, & \mathcal{X}_d(m) \neq \mathcal{X}_d(n) \end{cases} \end{aligned}$$

where $\mathcal{X}_d(n)$ is the n -th element of the set \mathcal{X}_d . In addition, we let γ^2 to be a very small number, e.g., 10^{-5} instead of $1/v_B^{\text{pri}}$ in the simulations and experiments, which yields an enhanced performance proven by our extensive simulations.

The remaining task is to derive the extrinsic mean and variance of Module B associated with the LMMSE denoiser (6). The extrinsic mean $\mathbf{x}_{B \rightarrow A}^{\text{ext}}$ is first constructed as the linear combination of $\mathbf{x}_B^{\text{post}}$ and $\mathbf{x}_B^{\text{pri}}$ with the form of (7b). Next, we determine coefficients α and c according to the divergence-free property of the series of algorithms extended from the Turbo signal recovery principle [33]. The details of this principle can be summarized in the following two conditions:

(a) The error of the input vector and extrinsic mean of Module B is orthogonal, namely,

$$E[(\mathbf{x}_B^{\text{pri}} - \mathbf{x})^T(\mathbf{x}_{B \rightarrow A}^{\text{ext}} - \mathbf{x})] = 0; \quad (12)$$

(b) The error of extrinsic mean of Module B $E[\|\mathbf{x}_{B \rightarrow A}^{\text{ext}} - \mathbf{x}\|^2]$ is minimized.

Finally, coefficients α and c satisfying conditions (a) and (b) can be obtained following the derivations in [34], which is given by

$$\alpha = \frac{\text{diag}(\mathbf{W}_{d,\text{LMMSE}})\text{diag}^{-1}(\mathbf{q}_d)\mathbf{1}_{N_d \times 1}}{N_d}, \quad (13a)$$

$$c = \frac{(\mathbf{x}_B^{\text{pri}})^H(\mathbf{x}_B^{\text{post}} - \alpha\mathbf{x}_B^{\text{pri}})}{\|\mathbf{x}_B^{\text{post}} - \alpha\mathbf{x}_B^{\text{pri}}\|^2}. \quad (13b)$$

In addition, we can approximate the extrinsic variance $v_{B \rightarrow A}^{\text{ext}} = \frac{1}{N} \|\mathbf{x}_{B \rightarrow A}^{\text{ext}} - \mathbf{x}\|^2$ by relaxing the exact \mathbf{x} as its estimate $\mathbf{x}_B^{\text{post}}$.

Notably, nearly all amplitude information is lost irretrievably under 1-bit quantization. We must recover the amplitude information, specifically the average channel gain $P_h = \frac{1}{N_d} \sum_{j \in \mathcal{X}_d} |h_j|^2$, by additional means to overcome this intrinsic defect of 1-bit ADC and further improve the performance. We refine the channel estimate $\hat{\mathbf{h}}_d$ with the extra amplitude information by operating channel normalization expressed by

$$\tilde{\mathbf{h}}_d = \sqrt{\hat{P}_h} \frac{\hat{\mathbf{h}}_d}{\|\hat{\mathbf{h}}_d\|}, \quad (14)$$

which is the final output of the channel estimator. In our system, the estimated P_h can be obtained from the current gain of AGC circuit g_{AGC} , which is defined by

$$\hat{P}_h = \left(\frac{1}{g_{\text{AGC}}} - \widehat{\sigma^2} \right) \times \frac{N}{N_d}. \quad (15)$$

We use $\bar{\mathbf{h}}_d = \sqrt{g_{\text{AGC}}} \tilde{\mathbf{h}}_d$ as the CSI for the data detector after obtaining the normalized channel estimate $\tilde{\mathbf{h}}_d$. The channel normalization is unnecessary when the ADC precision is more

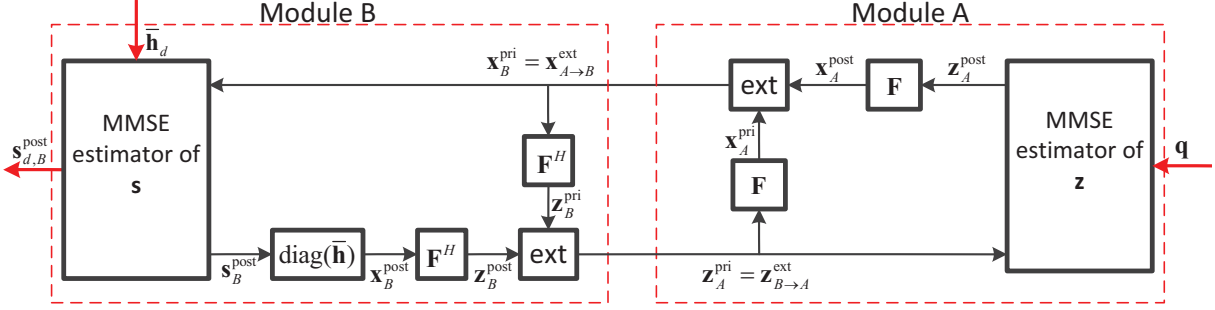


Fig. 4: Block diagram of GTurbo-based data detector with estimated CSI \bar{h} . The “ext” block represents the extrinsic information computation. The block of a certain matrix represents the operation of left-multiplying the input vector by the matrix in the block.

than 1 bit because the majority of amplitude information can be recovered by the proposed GTurbo-LMMSE channel estimator. This result can be verified by numerical results presented in Section IV. We let $\bar{h}_d = \sqrt{g_{\text{AGC}}} \hat{h}_d$ as the CSI for the data detector under the case without channel normalization.

D. Data Detector

The data detector is designed for computing the MMSE estimate of s and its corresponding MSE based on the quantized received signal \mathbf{q} modeled by (1). The GTurbo principle can be directly used for data detection by following the framework of [23, Algorithm 1] using the estimated channel parameters \bar{h} as the known CSI. In this subsection, we provide a brief introduction to this GTurbo-based detector. We define two auxiliary vectors similar to (3) as follows:

$$\mathbf{x} = \text{diag}(\mathbf{h})\mathbf{s}, \quad \mathbf{z} = \mathbf{F}^H \mathbf{x}.$$

The computation procedures are demonstrated in Algorithm 2, and the corresponding flow diagram of this algorithm is presented in Fig. 4. This detector has two modules as follows: Module A calculates the coarse estimation of \mathbf{x} without considering the prior distribution of \mathbf{s} ; Module B refines the estimate by considering the prior distribution of \mathbf{s} .

In Module A, (16a) and (16b) compute the posteriori mean and variance of z_j with explicit expressions provided by (8a) and (8b), respectively. The extrinsic variance of Module A can be computed using (17a) and (17b), while the extrinsic mean can be computed using (17c) and (17d), correspondingly. Algorithms 1 and 2 demonstrate the same operations in Module A, which can be implemented hardware-friendly using the hardware architecture proposed in [24]. Therefore, these algorithms can share the identical circuit module when implementing the application specific integrated circuit (ASIC) of the receiver in practice. In module B, we compute the estimate of \mathbf{s} and its MSE for $j \in \mathcal{X}_d$ in (18a) and (18b). Their explicit expressions are given by

$$s_{j,B}^{\text{post}} = \frac{\sum_{s \in \mathcal{S}} s \mathcal{CN} \left(s; \frac{x_{j,B}^{\text{pri}}}{\bar{h}_j}, \frac{v_B^{\text{pri}}}{|\bar{h}_j|^2} \right)}{\sum_{s \in \mathcal{S}} \mathcal{CN} \left(s; \frac{x_{j,B}^{\text{pri}}}{\bar{h}_j}, \frac{v_B^{\text{pri}}}{|\bar{h}_j|^2} \right)}, \quad (20a)$$

Algorithm 2: GTurbo-based Data Detector

Initialization: $\mathbf{z}_A^{\text{pri}} = \mathbf{0}_{N \times 1}$, $\mathbf{x}_B^{\text{pri}} = \mathbf{0}_{N \times 1}$, $\mathbf{x}_B^{\text{post}} = \mathbf{0}_{N \times 1}$,
 $v_A^{\text{pri}} = \frac{1}{N} \sum_{j \in \mathcal{X}_d} |\bar{h}_j|^2$;

for $t = 1 : T_{\text{max}}$ **do**

Module A:

(1) Compute the posteriori mean/variance of \mathbf{z} :

$$z_{j,A}^{\text{post}} = \mathbb{E} \left[z_j^R \mid q_j^R \right] + j \mathbb{E} \left[z_j^I \mid q_j^I \right], \quad (16a)$$

$$v_{j,A}^{\text{post}} = \text{var} \left[z_j^R \mid q_j^R \right] + \text{var} \left[z_j^I \mid q_j^I \right], \quad (16b)$$

(2) Compute the extrinsic mean/variance of \mathbf{x} :

$$v_A^{\text{post}} = \frac{1}{N} \sum_{j=1}^N v_{j,A}^{\text{post}}, \quad (17a)$$

$$v_B^{\text{pri}} = v_{A \rightarrow B}^{\text{ext}} = \left(\frac{1}{v_A^{\text{post}}} - \frac{1}{v_A^{\text{pri}}} \right)^{-1}, \quad (17b)$$

$$\mathbf{x}_{A \rightarrow B}^{\text{ext}} = v_{A \rightarrow B}^{\text{ext}} \left(\frac{\mathbf{F} \mathbf{z}_A^{\text{post}}}{v_A^{\text{post}}} - \frac{\mathbf{F} \mathbf{z}_A^{\text{pri}}}{v_A^{\text{pri}}} \right), \quad (17c)$$

$$\mathbf{x}_{d,B}^{\text{pri}} = \mathbf{x}_{d,A \rightarrow B}^{\text{ext}}, \quad (17d)$$

Module B:

(3) Compute the posteriori mean/variance of \mathbf{q} :

$$s_{j,B}^{\text{post}} = \mathbb{E} \left[s_j \mid \bar{h}_j, x_{j,B}^{\text{pri}} \right], \quad j \in \mathcal{X}_d, \quad (18a)$$

$$v_{j,B}^{\text{post}} = \text{var} \left[s_j \mid \bar{h}_j, x_{j,B}^{\text{pri}} \right], \quad j \in \mathcal{X}_d, \quad (18b)$$

(4) Compute the extrinsic mean/variance of \mathbf{z} :

$$v_B^{\text{post}} = \frac{1}{N_d} \sum_{j \in \mathcal{X}_d} |\bar{h}_j|^2 v_{j,B}^{\text{post}}, \quad (19a)$$

$$v_A^{\text{pri}} = v_{B \rightarrow A}^{\text{ext}} = \left(\frac{1}{v_B^{\text{post}}} - \frac{1}{v_B^{\text{pri}}} \right)^{-1}, \quad (19b)$$

$$x_{j,B}^{\text{post}} = \bar{h}_j s_{j,B}^{\text{post}}, \quad j \in \mathcal{X}_d, \quad (19c)$$

$$\mathbf{z}_A^{\text{pri}} = \mathbf{z}_{B \rightarrow A}^{\text{ext}} = v_B^{\text{ext}} \left(\frac{\mathbf{F}^H \mathbf{x}_B^{\text{post}}}{v_B^{\text{post}}} - \frac{\mathbf{F}^H \mathbf{x}_B^{\text{pri}}}{v_B^{\text{pri}}} \right). \quad (19d)$$

end

$$v_{j,B}^{\text{post}} = \frac{\sum_{s \in \mathcal{S}} |s|^2 \mathcal{CN} \left(s; \frac{x_{j,B}^{\text{pri}}}{\bar{h}_j}, \frac{v_B^{\text{pri}}}{|\bar{h}_j|^2} \right)}{\sum_{s \in \mathcal{S}} \mathcal{CN} \left(s; \frac{x_{j,B}^{\text{pri}}}{\bar{h}_j}, \frac{v_B^{\text{pri}}}{|\bar{h}_j|^2} \right)} - |s_{j,B}^{\text{post}}|^2. \quad (20b)$$

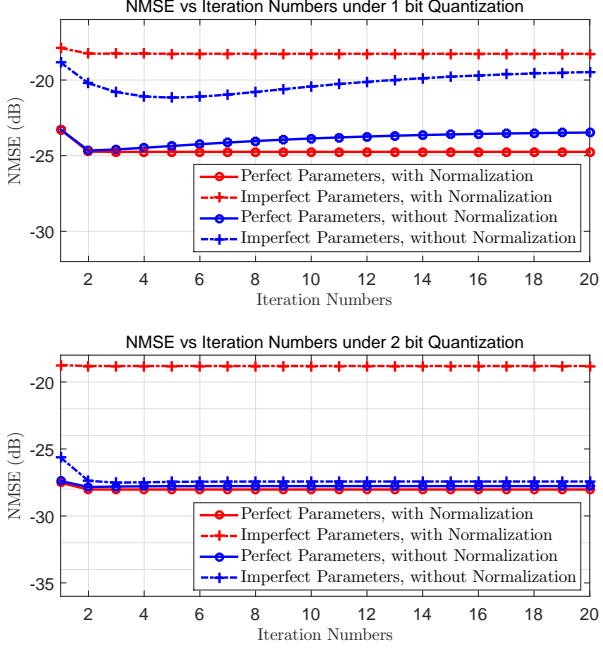


Fig. 5: NMSEs versus iteration numbers of the proposed GTurbo-LMMSE channel estimator (i.e., Algorithm 1) for the SNR of 12 dB and quantization precisions of 1 and 2 bit under four conditions.

where \mathcal{S} denotes the set of constellation points. Subsequently, we compute the extrinsic variance of Module B by (19a) and (19b) and extrinsic mean by (19c) and (19d). Further details are provided in [23].

The output of the GTurbo-based detector $s_{d,B}^{\text{post}}$ and $v_{d,B}^{\text{post}}$ is used for calculating the LLRs corresponding to each coded bits that are prepared for the subsequent Turbo decoding. We denote the i -th bit associated with the modulated symbol s_j by b_{ji} . The LLR of b_{ji} can be computed by [35]

$$\text{LLR}(b_{ji}) = \frac{1}{2\beta} \left(\left| s_{j,B}^{\text{post}} - s_{j,i}^+ \right|^2 - \left| s_{j,B}^{\text{post}} - s_{j,i}^- \right|^2 \right), \quad (21)$$

where $\beta = \frac{1}{N_d} \sum_{j \in \mathcal{X}_d} v_{j,B}^{\text{post}}$, $s_{j,i}^+$ and $s_{j,i}^-$ are defined as follows:

$$s_{j,i}^+ = \underset{s \in \mathcal{S}_i^+}{\operatorname{argmin}} \left| s - s_{j,B}^{\text{post}} \right|^2,$$

$$s_{j,i}^- = \underset{s \in \mathcal{S}_i^-}{\operatorname{argmin}} \left| s - s_{j,B}^{\text{post}} \right|^2,$$

where \mathcal{S}_i^+ and \mathcal{S}_i^- are the subset of the constellation symbols of the adopted modulation scheme, which i th bit is 1 and 0, respectively.

IV. NUMERICAL SIMULATIONS

In this section, we evaluate the performance of the proposed algorithms through numerical simulations, several relevant insights into those algorithms are also provided. The numerical simulations and OTA experiments share the following setting:

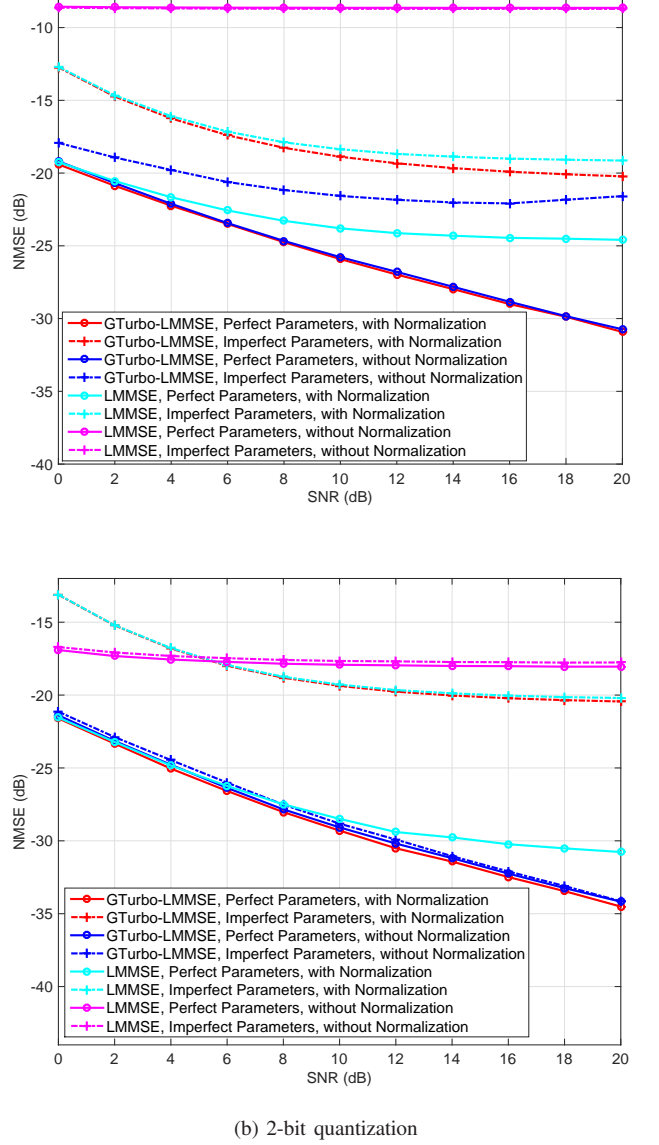
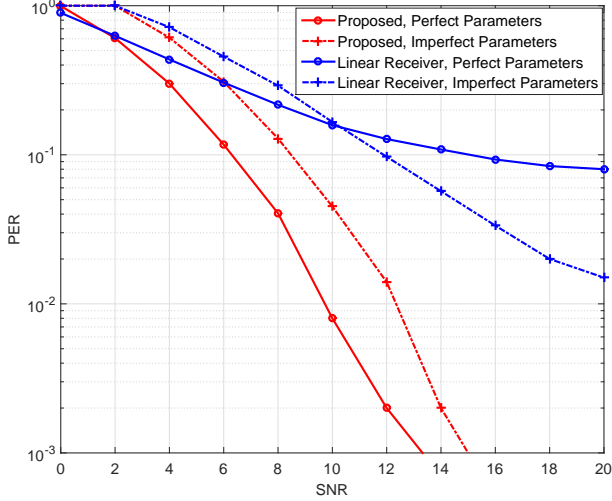


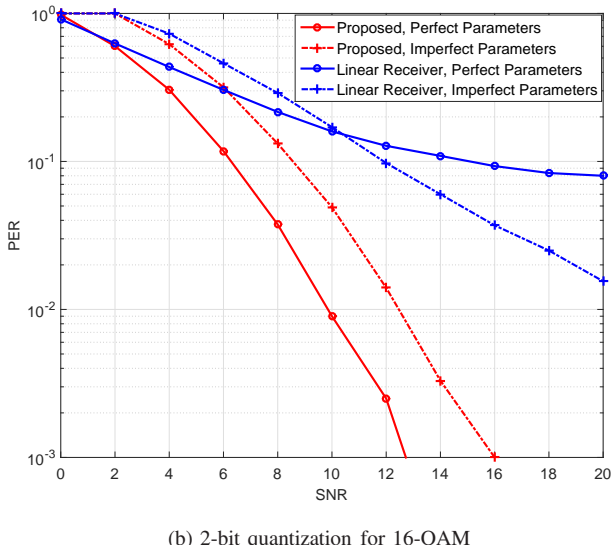
Fig. 6: NMSEs versus SNR of the proposed GTurbo-LMMSE channel estimator (i.e., Algorithm 1) and conventional LMMSE channel estimator under quantization precisions of 1 and 2 bit and four conditions.

the number of orthogonal subcarriers $N = 2048$, the number of subcarriers dedicated to data transmission $N_d = 1200$, the code rate is $1/3$, and each code word is transmitted in the successive three OFDM symbols. In this section, we simulate the channel using tapped delay line model with $L = 4$ channel taps, in which the power profile of each tag is set to 0, -7, -12, and -18 dB.

Each entry of the pilot symbols \mathbf{p}_d is drawn independently from the equiprobable 4-QAM constellation. We also normalize each entry of the pilot symbols \mathbf{p}_d and each entry of transmitted constellation symbols \mathbf{s}_d in which $E[|p_j|^2] = 1$ and $E[|s_j|^2] = 1$ for $j \in \mathcal{X}_d$. The desired performance metrics are obtained through the Monte-Carlo simulations of 1,000 independent channel realizations. We compare the



(a) 1-bit quantization for 4-QAM

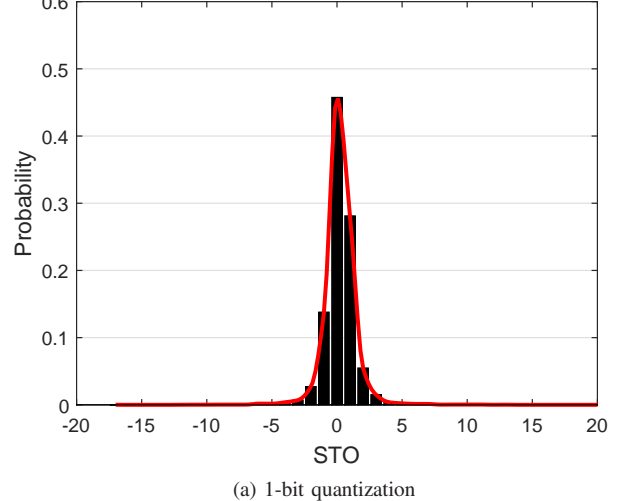


(b) 2-bit quantization for 16-QAM

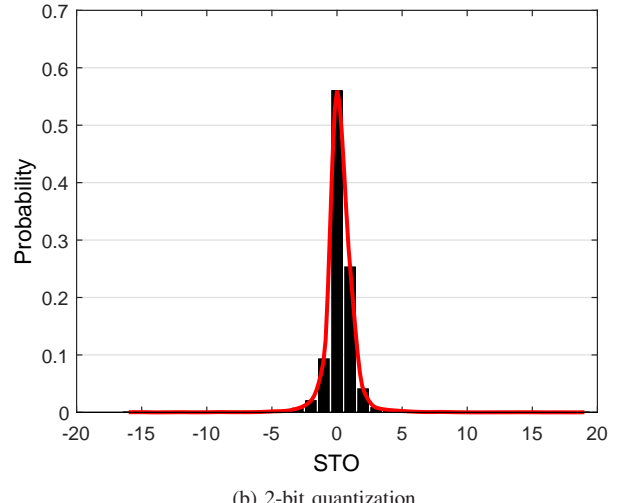
Fig. 7: PERs versus SNR of the proposed algorithms and linear receiver.

performance of the proposed algorithms with linear receiver algorithms, including conventional LMMSE channel estimator performed by left-multiplying $\mathbf{F}\mathbf{q}/\bar{\mathbf{p}}$ by the LMMSE weight matrix constructed as (11), and linear detector conducted by first approximating the quantized received signal (1) through the additive quantization noise model (AQNM) [36] and then computing the estimate of \mathbf{s} and its corresponding MSE based on the conventional one-tap equalizer.

In the following experiments, we discuss the influence of the channel normalization in (14) and the imperfect parameters, such as $g_{\text{AGC}} \neq 1/P_r$, $\sigma^2 \neq \bar{\sigma}^2$, and $\hat{L} \neq L$, on the performance of Algorithm 1. We artificially impose an error that is uniformly distributed in $[-30\%, 30\%]$ on parameters $1/P_r$ and σ^2 to obtain \hat{g}_{AGC} and $\hat{\sigma}^2$, and let $\hat{L} = 6$ to simulate the practical situation that exact parameters $1/P_r$, σ^2 and L are unavailable. Moreover, we let $\hat{g}_{\text{AGC}} = 1/P_r$, $\hat{\sigma}^2 = \sigma^2$, and $\hat{L} = L$ to simulate the ideal situation as



(a) 1-bit quantization



(b) 2-bit quantization

Fig. 8: Distribution of STO corresponding to the exact synchronization position.

a benchmark. The performances are compared under four conditions, namely, perfect parameters with normalization, perfect parameters without normalization, imperfect parameters with normalization, and imperfect parameters without normalization for each case of quantization precision and SNR in Figs. 5 and 6. Fig. 5 depicts the NMSEs of $\tilde{\mathbf{h}}_d$ defined as

$$\text{NMSE} = \frac{\|\tilde{\mathbf{h}}_d - \mathbf{h}_d\|^2}{\|\mathbf{h}_d\|^2}$$

which is obtained by Algorithm 1 versus the iteration numbers for the SNR of 12 dB and the quantization precisions of 1 and 2 bit under the aforementioned four conditions. The NMSE performance is better with perfect parameters than with imperfect parameters. We find that Algorithm 1 cannot converge without channel normalization with 1-bit ADC because nearly all amplitude information is lost under 1-bit quantization. Therefore, we cannot recover the lost amplitude information through the proposed iterative algorithm without extra information about the average channel gain P_h .

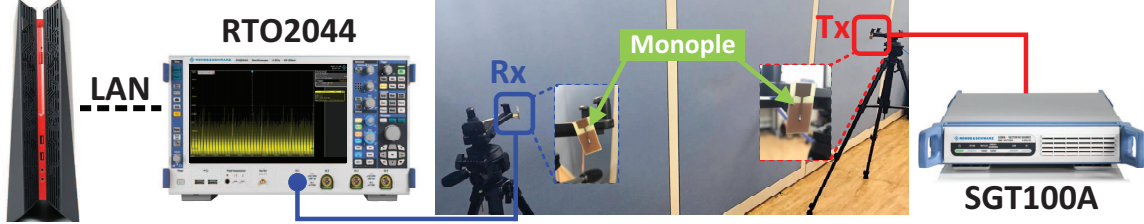


Fig. 9: Picture of the proposed prototyping system.

The NMSE performance with channel normalization is better than that without normalization, except for the case of 2-bit quantization with imperfect parameters. This result reflects that information about the average channel gain P_h recovered by Algorithm 1 is much better than that estimated by (15) from incorrect g_{AGC} and $\widehat{\sigma^2}$ provided that the quantization bit is larger than 1. The result demonstrates that channel normalization is unnecessary with quantization resolution of 2 bit and larger under which amplitude information can be recovered precisely through the proposed iterative algorithm when implementing the algorithms in practice.

Fig. 6 compares the NMSE performances of Algorithm 1 and the conventional LMMSE channel estimator under different quantization precisions and the four conditions. Generally, the proposed channel estimation algorithm outperforms the conventional LMMSE channel estimator for each case, because the conventional LMMSE channel estimator is designed highly relied on the orthogonality of the different subcarriers, which has been already destroyed by low-resolution ADCs. We also notice that the conventional LMMSE estimator without channel normalization undergoes a significant performance degradation compared with its performance with normalization, even under 2-bit quantization. This result verifies the extremely poor capability of the conventional LMMSE channel estimator to recover any amplitude information from low-resolution observations. Therefore, the results also reveal that the proposed GTurbo-LMMSE channel estimator has a robust capability for recovering channel amplitude information under the quantization precision of 2 bits.

Fig. 7 compares the overall information recovery performances in terms of the packet error rate (PER) between the combination of the proposed algorithms and the combination of linear schemes. For both cases, the PER obtained by the proposed algorithms is lower than 0.1 and reduces steeply when the SNR is more than 8 dB, which can be considered as achieving the reliable data transmission. However, obvious error floors appear for the PER performance of the linear receiver. Therefore, a significant performance gain can be obtained by using our proposed algorithms. We also find that imperfect parameters do not result in significant performance losses (with approximately 2 dB loss in SNR). This result can be attributed to the robust signal recovery capability of the proposed algorithms and error correction of Turbo code. We notice that an anti-intuitive phenomenon occurs for the linear receiver. Specifically, the performance with imperfect parameters outperforms that with perfect parameters under the SNR of more than 10 dB. This is because that the AQNM

cannot yield a satisfactory approximation to (1) under high SNR. Under this condition, imperfect parameters compensate minimally for the mismatch of the AQNM and result in this performance improvement. This result is a form of a special phenomenon called *stochastic resonance* [37].

Synchronization precision is also a critical performance metric for system implementation, except for the error-rate performance evaluated above. We display the distribution of different STOs corresponding to the exact starting point of each OFDM symbol under the SNR of 15 dB and quantization precision of 1–2 bit in Fig. 8. The exact synchronization position under extremely low quantization precision of 1 and 2 bits can be identified with the probability of approximately 0.45 and 0.56, respectively. The STO is retained within the range from -4 to 4 with the highest probability, which is an acceptable range of synchronization error. We can conclude from the above results that the conventional synchronization technique remains reliable for received samples with low-resolution quantization.

V. OTA EXPERIMENTS

In this section, we present the OTA experiment results to verify the reliability of our proposed Q-OFDM transmission scheme. We first establish a proof-of-concept prototyping system, which is depicted in Fig. 9. The transmitter and receiver are established with a separate baseband and RF processing unit. Baseband processing is performed through the software programmed in the host computers. The corresponding procedures have been specified in Sections II and III. The RF processing is conducted by using the Rohde & Schwarz components. Specifically, we use SGT100A for the transmitter and RTO2044 for the receiver. The output baseband samples of RTO2044 are quantized by high-resolution ADC. Thus, the coarse quantization is performed virtually by the software before being further processed. This setting allows us to obtain certain reference parameters for the subsequent performance evaluations. The data exchange between the baseband processing software and RF processing components is performed through off-the-shelf high-speed interfaces.

The frame structure used in our prototyping system is illustrated in Fig. 10. This structure is designed based on the frame structure of the long-term evolution system, which can be flexibly reconfigured for future extensions. An entire radio frame consists of 10 subframes; each subframe has two consecutive slots. In each slot, seven OFDM symbols are transmitted. In our system, L_{cp} is set to 144 for OFDM symbols 1–6, and 160 for OFDM symbol 0 in each slot. For

TABLE I: 4-QAM under 1 bit quantization

Transmitted Power (dBm)	Distance (cm)	SNR (dB)	MSE (dB)	Uncoded BER	Coded BER	PER
-10	50	21.9369	-26.2585	0	0	0.0241
	100	14.7147	-21.7561	0	0	0.0550
	200	9.0586	-17.6597	0.5925	0.0067	0.1225
0	200	16.9047	-17.4163	0.0050	1.5308×10^{-5}	0.0646
	500	14.6274	-17.8153	0.0138	5.4899×10^{-5}	0.0831

TABLE II: 16-QAM under 2 bit quantization

Transmitted Power (dBm)	Distance (cm)	SNR (dB)	MSE (dB)	Uncoded BER	Coded BER	PER
-10	50	21.7440	-29.4138	0	0	0.0529
	100	15.0625	-25.4841	0	0	0.0810
	200	9.4999	-19.6486	0.5025	0.0033	0.1556
0	200	17.5740	-19.5718	0.0141	7.1527×10^{-5}	0.0796
	500	14.7362	-19.0786	0.0213	7.8442×10^{-4}	0.0950

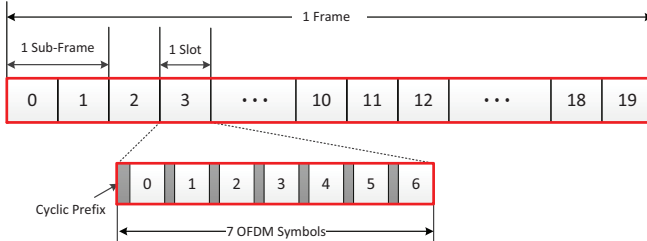


Fig. 10: Frame structure

each frame, slots 2–19 are dedicated for data transmission, in which the predefined pilot sequence is transmitted via the first OFDM symbol of these slots for channel estimation, while the rest of the six OFDM symbols are used for transmitting data sequences. To establish the synchronization between the transmitter and the receiver, OFDM symbol 6 of slots 0 to 10 are reversed for transmitting the primary synchronization signals (PSS). The first OFDM symbol of slot 1 is padded by null symbols for noise power estimation.

TABLE III: System Parameters

Parameter	Value
System Bandwidth	100 MHz
Sampling Rate	153.6 MHz
Subcarrier Interval	75 KHz
Frame Duration	2 ms
Subframe Duration	0.2 ms
OFDM symbol Duration (without CP)	13.33 μ s

The experiments are conducted in an indoor environment displayed in Fig. 11. The transmitter and receiver are placed in the corridor beside office table. We adjust their distance by fixing the transmitter and placing the receiver in different positions. In our experiments, the carrier frequency is set to 3.5 GHz, and we extend the bandwidth to 100 MHz to support a high data transmission with unchanged frame duration. The resulting system parameters are listed in Table

III. Experiments are conducted to evaluate the error-rate performance of the proposed prototyping system under different quantization precisions and modulation schemes including 1 bit for 4-QAM and 2 bits for 16-QAM. Various average SNRs are generated by changing the transmit power and distance between transmitter and receiver. The performance metrics to be evaluated include the MSE of estimated channel parameter, coded and uncoded BER, and PER of the information bits in each code word. The average SNRs and these metrics are measured from 10,000 received frames and obtained by taking the average of these measured results. We use the LMMSE channel estimate from the high-resolution received signal as the reference when calculating the MSE of estimated channel parameters. The experiment results are shown in Tables I and II, which present the measured performance metrics when transmitting 4-QAM with 1-bit quantization and 16-QAM with 2-bit quantization, respectively. We can conclude that the reliable data transmission can be guaranteed with a SNR that is higher than 10 dB for both cases.

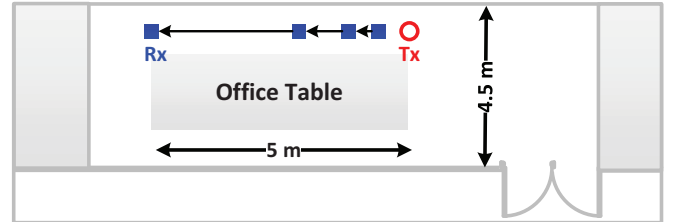


Fig. 11: The experiment environment and equipment deployment.

VI. CONCLUSION

This paper proposed an overall system architecture for supporting a reliable OFDM transmission with ultra-low resolution ADC (i.e., 1–2 bit) at the receiver. We developed a novel GTurbo-LMMSE channel estimator by aligning Module A of the GTurbo framework with the LMMSE denoiser to

estimate the desired channel parameters without their priori distribution. Synchronization, AGC and noise power estimation were also considered and integrated into the system design, except for the novel inference algorithms. We established the first prototyping system based on extremely low-resolution quantization at the receiver worldwide. OTA experiments were conducted to examine the reliability of the proposed system. The following conclusions were drawn from the results of numerical simulations and OTA experiments.

- The proposed GTurbo-LMMSE channel estimator outperforms the conventional LMMSE channel estimator in terms of NMSE performance and amplitude recovery capability. In addition, Channel normalization is indispensable with 1-bit ADC.
- The GTurbo-based detector in cooperation with the proposed GTurbo-LMMSE channel estimator obtain significant gain in error-rate performance compared with the linear schemes, which is insufficient for dealing with the strong nonlinear distortion caused by low-resolution ADCs.
- The precision of the synchronization searching can be guaranteed even from coarsely quantized received signals.
- A communication system supporting reliable OFDM transmission with ultra-low resolution ADCs was achieved.

REFERENCES

- [1] R. Walden, "Analog-to-digital converter survey and analysis," *IEEE J. Sel. Areas Commun.*, vol. 17, no. 4, pp. 539–550, Apr. 1999.
- [2] B. Murmann. ADC performance survey 1997-2017. [Online]. Available: <http://web.stanford.edu/~murmann/adcsurvey.html>
- [3] A. Mezghani and J. Nossek, "Analysis of rayleigh-fading channels with 1-bit quantized output," in *Proc. IEEE Int. Symp. Inf. Theory (ISIT)*, Toronto, Canada, Jul. 2008, pp. 260–264.
- [4] J. Singh, O. Dabeer, and U. Madhow, "On the limits of communication with low-precision analog-to-digital conversion at the receiver," *IEEE Trans. Commun.*, vol. 57, no. 12, pp. 3629–3639, Dec. 2009.
- [5] S. Krone and G. Fettweis, "Fading channels with 1-bit output quantization: Optimal modulation, ergodic capacity and outage probability," in *Proc. IEEE Information Theory Workshop (ITW)*, Dublin, Ireland, 2010, pp. 1–5.
- [6] J. Mo and R. Heath, "Capacity analysis of one-bit quantized MIMO systems with transmitter channel state information," *IEEE Trans. Signal Process.*, vol. 63, no. 20, pp. 5498–5512, Oct. 2015.
- [7] N. Liang and W. Zhang, "Mixed-ADC massive MIMO uplink in frequency-selective channels," *IEEE Trans. Commun.*, vol. 64, no. 11, pp. 4652–4666, Nov. 2016.
- [8] L. Fan, S. Jin, C.-K. Wen, and H. Zhang, "Uplink achievable rate for massive MIMO systems with low-resolution ADC," *IEEE Commun. Lett.*, vol. 19, no. 12, pp. 2186–2189, Dec. 2015.
- [9] S. Rini, L. Barletta, Y. Eldar, and E. Erkip, (2017) A general framework for low-resolution receivers for MIMO channels. [Online]. Available: <https://arxiv.org/abs/1702.08133v1>
- [10] C. Risi, D. Persson, and E. G. Larsson, (2014) Massive MIMO with 1-bit ADC. [Online]. Available: <http://arxiv.org/abs/1404.7736>
- [11] A. Mezghani, M.-S. Khoufi, and J. Nossek, "A modified MMSE receiver for quantized MIMO systems," in *Proc. ITG Workshop Smart Antennas (WSA)*, 2007.
- [12] J. Choi, J. Mo, and R. Heath, "Near maximum-likelihood detector and channel estimator for uplink multiuser massive MIMO systems with one-bit ADCs," *IEEE Trans. Commun.*, vol. 64, no. 5, pp. 2005–2018, May 2016.
- [13] Y.-S. Jeon, S.-N. Hong, and N. Lee, (2017) Uplink multiuser massive MIMO systems with low-resolution ADCs: A coding-theoretic approach. [Online]. Available: <https://arxiv.org/abs/1704.03287v1>
- [14] ——, (2017) Supervised-learning-aided communication framework for massive MIMO systems with low-resolution ADCs. [Online]. Available: <https://arxiv.org/abs/1610.07693v3>
- [15] A. Mezghani and J. Nossek, "Belief propagation based mimo detection operating on quantized channel output," in *Proc. IEEE Int. Symp. Inf. Theory (ISIT)*, Austin, TX, 13–18 June 2010, pp. 2113–2117.
- [16] T. Zhang, C.-K. Wen, S. Jin, and T. Jiang, "Mixed-ADC massive MIMO detectors: Performance analysis and design optimization," *IEEE Trans. Wireless Commun.*, vol. 15, no. 11, pp. 7738–7752, Nov. 2016.
- [17] C.-K. Wen, C.-J. Wang, S. Jin, K.-K. Wong, and P. Ting, "Bayes-optimal joint channel-and-data estimation for massive MIMO with low-precision ADCs," *IEEE Trans. Signal Process.*, vol. 64, no. 10, pp. 2541–2556, May 2016.
- [18] J. G. Proakis, *Digital Communications*. Boston, USA: McGraw-Hill Companies, 2007.
- [19] *IEEE Std 802.11ad-2012 (Amendment to IEEE Std 802.11-2012)*, Std., 2012.
- [20] C. Molln, J. Choi, E. G. Larsson, and R. Heath, "One-bit ADCs in wideband massive MIMO systems with OFDM transmission," in *Proc. 2016 IEEE International Conference on Acoustics, Speech and Signal Processing (ICASSP)*, March 2016, pp. 3386–3390.
- [21] C. Studer and G. Durisi, "Quantized massive MU-MIMO-OFDM uplink," *IEEE Trans. Commun.*, vol. 64, no. 6, pp. 2387–2399, June 2016.
- [22] J. García, J. Munir, K. Roth, and J. A. Nossek, Channel estimation and data equalization in frequency-selective MIMO systems with one-bit quantization. 2016. [Online]. Available: <http://arxiv.org/abs/1504.04799v1>,preprint.
- [23] H. Wang, C. K. Wen, and S. Jin, "Bayesian optimal data detector for mmwave OFDM system with low-resolution ADC," *IEEE J. Sel. Areas Commun.*, vol. 35, Sept. 2017.
- [24] J. Yang, C. Zhang, S. Jin, C.-K. Wen, and X. You, "Efficient hardware architecture for compressed sensing with DFT sensing matrix," in *Proc. IEEE International Workshop on Signal Processing Systems (SiPS)*, Oct. 26–28, 2016, pp. 207–212.
- [25] O. Castañeda, S. Jacobsson, G. Durisi, M. Coldrey, T. Goldstein, and C. Studer, 1-bit massive MU-MIMO precoding in VLSI. 2017. [Online]. Available: <http://arxiv.org/abs/1702.03449>,preprint.
- [26] T. Liu, C.-K. Wen, S. Jin, and X. You, "Generalized Turbo signal recovery for nonlinear measurements and orthogonal sensing matrices," in *Proc. IEEE Int. Symp. Inf. Theory (ISIT)*, Barcelona, Spain, Jul. 10–15, 2016, pp. 2883–2887.
- [27] T. Blu and F. Luisier, "The sure-let approach to image denoising," *IEEE Trans. Image Process.*, vol. 16, no. 11, pp. 2778–2786, Nov. 2007.
- [28] K. Dabov, A. Foi, V. Katkovnik, and K. Egiazarian, "Image denoising with block-matching and 3d filtering," vol. 6064, 2006.
- [29] M. Elad and M. Aharon, "Image denoising via sparse and redundant representations over learned dictionaries," *IEEE Trans. Image Process.*, vol. 15, no. 12, pp. 3736–3745, Dec. 2006.
- [30] J.-F. Cai, E. J. Candès, and Z. Shen, "A singular value thresholding algorithm for matrix completion," *SIAM Journal on Optimization*, vol. 20, no. 4, pp. 1956–1982, 2010.
- [31] X. Yang, W. Lv, N. Wang *et al.* (2016) Design and implementation of a TDD-based 128-antenna massive MIMO prototyping system. [Online]. Available: <https://arxiv.org/abs/1608.07362>
- [32] O. Edfors, M. Sandell, J. J. van de Beek, S. K. Wilson, and P. O. Borjesson, "OFDM channel estimation by singular value decomposition," *IEEE Trans. Commun.*, vol. 46, no. 7, pp. 931–939, July 1998.
- [33] J. Ma and P. Li, "Orthogonal AMP," *IEEE Access*, vol. 5, pp. 2020–2033, 2017.
- [34] Z. Xue, J. Ma, and X. Yuan, "Denoising-based Turbo compressed sensing," *IEEE Access*, vol. 5, pp. 7193–7204, 2017.
- [35] Y. S. Cho, J. Kim, W. Y. Yang, and C. G. Kang, *MIMO-OFDM Wireless Communications With MATLAB*. Hoboken, NJ: Wiley, 2007.
- [36] O. Orhan, E. Erkip, and S. Rangan, "Low power analog-to-digital conversion in millimeter wave systems: Impact of resolution and bandwidth on performance," in *Proc. Information Theory and Applications Workshop (ITA)*, San Diego, USA, Feb. 1–6, 2015, pp. 191–198.
- [37] M. D. McDonnell, N. G. Stocks, C. E. M. Pearce, and D. Abbott, *Stochastic resonance: from suprathreshold stochastic resonance to stochastic signal quantization*. Cambridge University Press, 2008.